

Potential Safe Termination by Injection of Polypropylene Pellets in JET

GL Schmidt(*), S Ali-Arshad, D Bärlett, A Chankin, S Clement,
M Gadeberg, P Kupschus, D O'Brien, R Reichle, G Sadler, A Tanga
JET Joint Undertaking, Abingdon, Oxfordshire, OX14 3EA, UK

(*), Princeton Plasma Physics Laboratory, Princeton University, Princeton NJ, USA

RECEIVED
OCT 18 1995
OSTI

1.0 Introduction: Thermal energy and the magnetic field energy associated with the plasma current must be dissipated safely when a tokamak discharge is terminated in a disruption(1)(2). Magnetic energy can be dissipated by impurity radiation if position control is maintained(3). Prior to the dissipation of magnetic energy, thermal energy is usually conducted to the plasma contact points on a 1ms time scale in a thermal quench (1). A resistive, highly radiating plasma formed prior to the thermal quench, might dissipate both the thermal and magnetic energy by radiation minimizing damage due to local deposition. High speed injection of a low Z material can produce a resistive, highly radiating plasma on a 1ms time scale. Neon has recently been used in such an application on JT60-U (4). A large carbon pellet producing dilution temperatures $<1\text{keV}$ is a possible alternative. This paper summarizes the results of an initial experiment performed in JET using carbon injected at high speed, as a 6mm polypropylene pellet, to investigate this potential approach to a safe plasma termination.

2.0 Scenario: A 2MA, x-point plasma with toroidal field of 2.7T, $b/a=1.6$ and $q_{95}\sim 4$ formed the pellet target. The discharge was heated by NBI (4.3MW), ICRF (4.4MW) and

Lower Hybrid (1.5MW) producing a thermal energy content of 2.6MJ, a $T_e(0) = 3.8\text{keV}$ at $n_e(0) \sim 3.9 \times 10^{19} \text{ m}^{-3}$ and $N_e(\text{Total}) = 3 \times 10^{21}$. Pellet size and carbon content were matched to this target plasma within the constraints of the JET two stage high speed injector (5). A 3mm long x 6mm diameter, 70milli-gram polypropylene pellet was used with carbon and hydrogen fractions of 86% and 14%, total carbon $N_C \sim 4 \times 10^{21}$, and total electrons $N_e \sim 3 \times 10^{22}$. The pellet was injected during heating at 13.426s, speed 1200m/s,, reaching the plasma center in 700 μsec . Figures 1 - 3 present the time evolution of discharge parameters during the subsequent $\sim 25\text{ms}$ current decay. Four phases are identified.

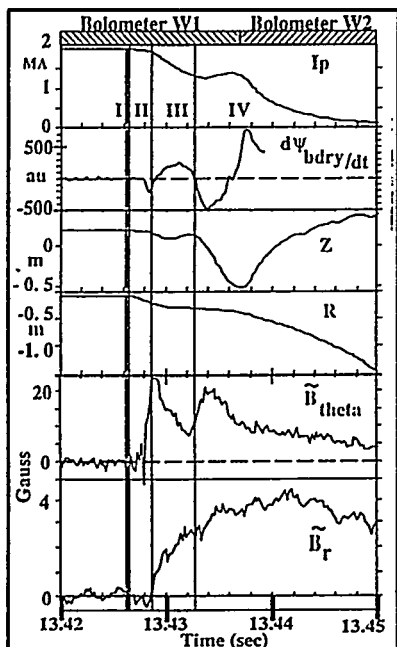


Figure 1: Plasma current (I_p), $d\psi/dt$ of boundary flux ($d\psi/dt$), Vertical (Z), and Radial Position (R), Perturbation of Poloidal Field at Wall and of Radial Field outside the Wall. Four phases: (I) Pellet Entry (II) Loss of Thermal Energy (III) Initial Current Decay (IV) Completion of Current Decay

2.1 Phase I: Carbon plasma formed. If the pellet were deposited uniformly the average electron deposition would be $3.8 \times 10^{20} \text{ m}^{-3}$. Since the pellet reaches the plasma center it is not certain that its entire mass is ablated. Deposition is estimated from the change in electron temperature at injection neglecting radiation losses during ablation. However, because the cutoff density for ECE is $\sim 1 \times 10^{20} \text{ m}^{-3}$ in this experiment and radiation is neglected, the analysis must be treated with caution. The measured temperature immediately following the collapse of the core is taken to be the dilution temperature

DISCLAIMER

This report was prepared as an account of work sponsored by an agency of the United States Government. Neither the United States Government nor any agency thereof, nor any of their employees, makes any warranty, express or implied, or assumes any legal liability or responsibility for the accuracy, completeness, or usefulness of any information, apparatus, product, or process disclosed, or represents that its use would not infringe privately owned rights. Reference herein to any specific commercial product, process, or service by trade name, trademark, manufacturer, or otherwise does not necessarily constitute or imply its endorsement, recommendation, or favoring by the United States Government or any agency thereof. The views and opinions of authors expressed herein do not necessarily state or reflect those of the United States Government or any agency thereof.

DISCLAIMER

Portions of this document may be illegible in electronic image products. Images are produced from the best available original document.

assuming the ablated mass toroidal transit time is sufficient to separate the temperature and density perturbation at the location of the measurement. The insert to figure 2a displays the measured core temperature at high time resolution. A dilution temperature of 0.5keV is obtained, then some 200 μ sec later the high density plasma deposited by the pellet is assumed to reach the detector, some 120 degrees in toroidal angle from the injector, and the ECE is cutoff causing the apparent additional temperature drop. Taking the temperature immediately following the central collapse at each radius as a local dilution temperature we infer a final electron density on axis of $<3 \times 10^{20} \text{ m}^{-3}$ and a total electron deposition of $<1.1 \times 10^{22}$. Assuming carbon to have lost 4 electrons consistent with coronal equilibrium at this final temperature (6) gives a carbon deposition of $<2.8 \times 10^{21}$ roughly 70% of the pellet.

2.2 Phase II: Loss of thermal energy occurs accompanied by slight current decay. The thermal loss is indicated by loss of plasma β in the EFIT equilibrium analysis and the resulting radial shift of the plasma. Radial position moves some 25cm. Ion energy loss on this same time scale is consistent with the observed drop in plasma neutron rate (insert 2c). Vertical position is unchanged. A perturbation in poloidal and radial field appears and grows but only to moderate amplitude. A strong non-thermal ECE burst is observed perhaps associated with the use of LH heating in the pre-pellet target. Such a burst can be detected even in the presence of a cutoff layer due to wall reflections and is often seen in low density disruptions. A negative

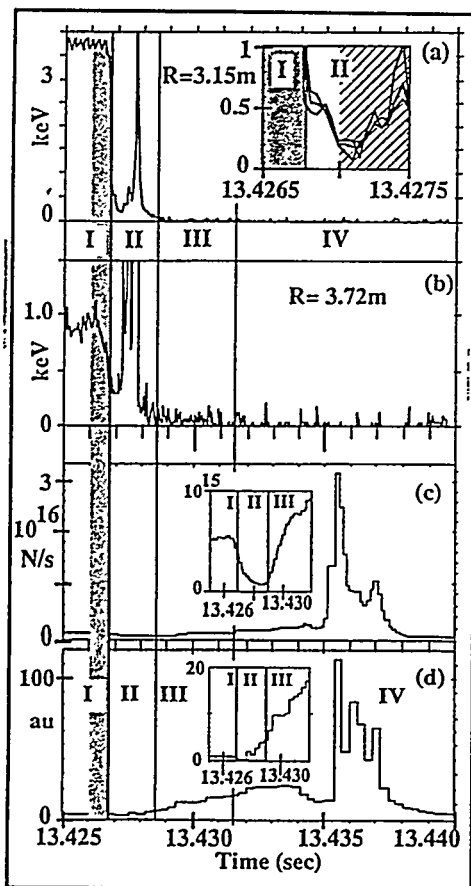


Figure 2: T_e from ECE at 3.16m (center) and 3.72m (edge) - (a) and (b). Insert at 3.03, 3.09, 3.16, 3.25m. Neutron rate-fission chamber (c). Hard x-ray - NaI scintillator (d).

$d\psi/dt$ spike is observed of 1ms duration. Current decreases by ~ 100 kA.

2.3 Phase III: Current decay rate increases; vertical position is maintained. Growth of the perturbed magnetic field is essentially complete and amplitude remains modest. Decay rate of ~ 200 kA/ms corresponds to a Spitzer resistance temperature of ~ 15 eV. At the boundary $d\psi/dt$ becomes positive. A steady increase in hard x-ray and neutron rates is observed indicating a gradual buildup of non-thermal electrons during the initial current decay. The rapid initial increase in x-ray and neutron emission rate immediately following the loss of thermal energy (fig 2c,d insert) is the start of this buildup. Plasma equilibria obtained up to ~ 6 ms after pellet entry using the EFIT equilibrium reconstruction code (7) are similar through the loss of thermal energy and little changed during the initial current decay from 2MA to 1.3MA. The x-point configuration is maintained with the separatrix contact points shifting only later in phase III. Elongation has decreased to 1.46 at the end of phase III. The q_{95} has increased. The plasma does not appear to contact the inner wall in either post pellet equilibrium. Vertical position control switches off near the end of phase III.

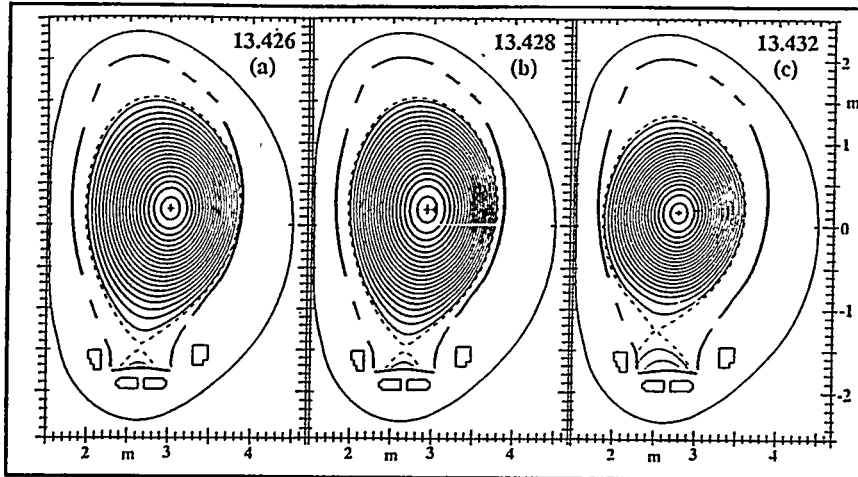


Figure 3: Plasma equilibrium (a) prior to the pellet event at 13.426s, (b) during phase II at 13.428s and (c) at the end of phase III at 13.432

2.4 Phase IV: Current termination. Current first increases by some 400kA above a simple extension of resistive decay and is accompanied by negative $d\psi/dt$. Near the maximum in vertical displacement a loss of non-thermal particles occurs (hard x-ray and photo-neutron burst). The current decay rate

then returns to $\sim 200\text{kA/ms}$, the plasma Z position returns to near the vessel center, and the discharge terminates on the inner wall. Vessel force is modest and displacement small and symmetric ($\sim 1\text{mm}$).

3.0 Energy Deposition: Figures 4 and 5 examine energy loss locally to divertor tiles and by radiation. The total energy available can be estimated from the sum of the internal and external magnetic energy, $\sim 4.5\text{MJ} + \sim 5.6\text{MJ}$, assuming all of the internal and 70% of external energy is coupled to the plasma, combined with the thermal energy $\sim 2.6\text{MJ}$. The thermal energy represents 20% of this total and 30% of the energy available during the first bolometer frame, W1 discussed in section 3.2.

3.1 Divertor Heat Deposition is inferred from divertor tile temperature (8). Localized power flow near the separatrix is observed in the two frames prior to the current decay. In the current decay frame a strong bremsstrahlung component is present but the separatrix signatures are still distinct. The peak temperatures are not strongly increased by any thermal quench. Integrated power flow to the tiles during the short period of the thermal energy loss can be estimated from a simple 1-D model by converting peak temperatures in the current decay frame to a total photon count. Temperatures in the preceding frame serve as an initial condition and separatrix geometry is presumed unchanged during the 2ms period. The measured temperatures indicate that less than 20% of the 2.6MJ thermal energy was deposited on the tiles assuming this was the only energy source.

3.2 Energy Dissipated by Radiation is measured using a multichord bolometer system from which the spacial distribution of radiation can be reconstructed

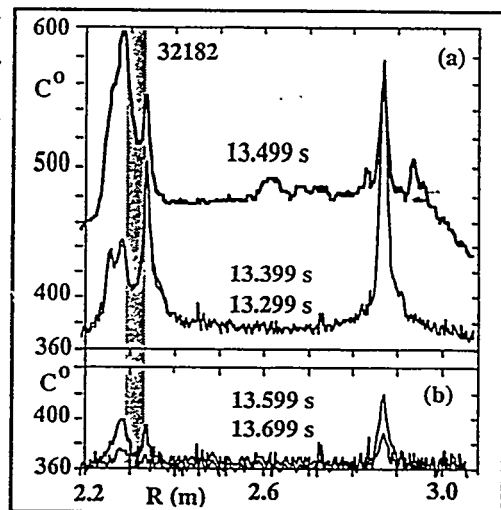


Figure 4: Divertor tile temperature. 100ms integration. Frames 13.299s and 13.399s before pellet injection. Frame 13.499s pellet event and subsequent current decay. Frames 13.599s and 13.699s show cooling of the tiles and detector background levels following termination of the discharge. Noise equivalent temperature 360 C. Shaded region indicates partial obstruction of detector line of sight.

using the ADMT method (9). Reconstruction of frame W1 uses detectors located at, and 2m from, the point of pellet injection. A few detectors view a portion of the pellet trajectory. Local radiation associated with the pellet ablation event has been removed by comparison with other detectors. This local radiation is large and may play a role in dissipation of the thermal energy. The reconstruction should be taken to reflect only the general character of the symmetric radiation. Radiation from throughout the plasma volume during frame W1 is clear and in marked contrast to the concentration of the radiation in the divertor region for the pre disruption frame. The pattern suggests only modest power flow to the divertor near the inner strike zone. Assuming toroidal symmetry, energy dissipated by radiation during the current termination is estimated to be $\sim 5.6\text{MJ}$ in period W1 and $\sim 2.4\text{MJ}$ in period W2.

4.0 Discussion: The pellet initiated resistive quench of the JET plasma current produced only moderate MHD activity. Growth of a non-thermal current was observed and experiments using additional pellets to suppress this current should be attempted. Simple coronal equilibrium estimates of carbon radiation immediately following pellet injection are in the range of 100MW to 500MW, suggesting additional effects play a role in dissipation of the thermal energy on a 2ms time scale. Simple extension to ITER of the experiment would call for use of a pellet containing perhaps 30X the electron content of the plasma to produce a dilution temperature of 500eV and with a speed $> 3\text{km/s}$ to reach the plasma center in $< 1\text{ms}$. In order to reduce these pellet requirements, to test the assumptions made in this analysis and to understand the radiation process more completely, experiments incorporating detailed measurement of radiated and conducted power at high time resolution should be carried out with pellets of similar and decreasing carbon content.

Discussions with P Noll, G Sannazzaro, G Sips,

B J Tubbing, M Verrecchia and J Wesson are gratefully acknowledged. GLS is supported by U.S. DoE Contract No. DE-AC02-76-CHO-3073

1- JA Wesson RD Gill, M Hugon et al. NF Vol. 29 (1989), p641.

2 - TFR Group NF Vol. 25 (1985), p 919.

3-K Yamazaki, GL Schmidt, NF Vol. 24 (1984), p445.

4- R Yoshino, et al CN-60-II-2, IAEA Seville 1994.

5-P Kupschus, K Sonnenberg, W Bailey et al. 16th Symposium on Fusion Technology, London (1990) Vol 1 p268.

6 -DE Post, RV Jensen, CB Tarter et al Atomic Data and Nuclear Data Tables Vol. 20 (1977).

7 - DP O'Brien, LL Lao, ER Solano et al. NF Vol. 32 (1992) p1351.

8 - S Clement, DJ Campbell, A Chankin et al 22nd EPS Bournemouth, UK 1995.

9 - J.C. Fuchs et. al., 21st EPS Montpellier, France 1994.

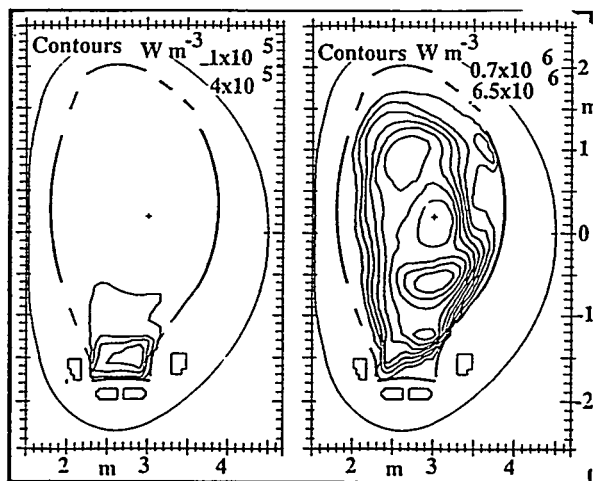


Figure 5 Reconstruction of radiated power, 20ms integration. Left frame, prior to pellet injection. Right frame, thermal loss and early current decay window W1 (figure 1). Note that the contour ranges differ in the two frames.